



Time-Dependent CP -Violating Asymmetries in $b \rightarrow s\bar{q}q$ Transitions

K.-F. Chen,²⁴ F. Fang,⁶ A. Garmash,³³ K. Hara,⁷ M. Hazumi,⁷ T. Higuchi,⁷ H. Kakuno,⁴³
A. Kusaka,⁴³ T. Shibata,²⁷ O. Tajima,⁷ K. Trabelsi,⁶ T. Ziegler,³³ K. Abe,⁷ K. Abe,⁴¹
H. Aihara,⁴³ Y. Asano,⁴⁷ T. Aushev,¹¹ S. Bahinipati,⁴ A. M. Bakich,³⁸ Y. Ban,³²
E. Barberio,¹⁹ M. Barbero,⁶ A. Bay,¹⁶ I. Bedny,¹ U. Bitenc,¹² I. Bizjak,¹² S. Blyth,²⁴
A. Bondar,¹ A. Bozek,²⁵ M. Bračko,^{7,18,12} J. Brodzicka,²⁵ T. E. Browder,⁶ P. Chang,²⁴
Y. Chao,²⁴ A. Chen,²² W. T. Chen,²² B. G. Cheon,³ R. Chistov,¹¹ S.-K. Choi,⁵ Y. Choi,³⁷
Y. K. Choi,³⁷ A. Chuvikov,³³ J. Dalseno,¹⁹ M. Danilov,¹¹ M. Dash,⁴⁸ L. Y. Dong,⁹
A. Drutskoy,⁴ S. Eidelman,¹ Y. Enari,²⁰ S. Fratina,¹² N. Gabyshev,¹ T. Gershon,⁷
G. Gokhroo,³⁹ B. Golob,^{17,12} A. Gorišek,¹² J. Haba,⁷ T. Hara,³⁰ H. Hayashii,²¹ L. Hinz,¹⁶
T. Hokuue,²⁰ Y. Hoshi,⁴¹ S. Hou,²² W.-S. Hou,²⁴ Y. B. Hsiung,²⁴ T. Iijima,²⁰ A. Imoto,²¹
K. Inami,²⁰ A. Ishikawa,⁷ H. Ishino,⁴⁴ R. Itoh,⁷ M. Iwasaki,⁴³ Y. Iwasaki,⁷ J. H. Kang,⁴⁹
J. S. Kang,¹⁴ P. Kapusta,²⁵ S. U. Kataoka,²¹ N. Katayama,⁷ H. Kawai,² T. Kawasaki,²⁷
H. R. Khan,⁴⁴ H. Kichimi,⁷ H. J. Kim,¹⁵ S. M. Kim,³⁷ K. Kinoshita,⁴ S. Korpar,^{18,12}
P. Križan,^{17,12} P. Krokovny,¹ S. Kumar,³¹ C. C. Kuo,²² A. Kuzmin,¹ Y.-J. Kwon,⁴⁹
G. Leder,¹⁰ S. E. Lee,³⁶ T. Lesiak,²⁵ J. Li,³⁵ S.-W. Lin,²⁴ D. Liventsev,¹¹ G. Majumder,³⁹
F. Mandl,¹⁰ D. Marlow,³³ T. Matsumoto,⁴⁵ A. Matyja,²⁵ Y. Mikami,⁴² W. Mitaroff,¹⁰
K. Miyabayashi,²¹ H. Miyake,³⁰ H. Miyata,²⁷ R. Mizuk,¹¹ T. Nagamine,⁴² Y. Nagasaka,⁸
I. Nakamura,⁷ E. Nakano,²⁹ M. Nakao,⁷ Z. Natkaniec,²⁵ S. Nishida,⁷ O. Nitoh,⁴⁶
S. Noguchi,²¹ T. Nozaki,⁷ S. Ogawa,⁴⁰ T. Ohshima,²⁰ T. Okabe,²⁰ S. Okuno,¹³ S. L. Olsen,⁶
Y. Onuki,²⁷ W. Ostrowicz,²⁵ P. Pakhlov,¹¹ H. Palka,²⁵ C. W. Park,³⁷ H. Park,¹⁵
N. Parslow,³⁸ L. S. Peak,³⁸ R. Pestotnik,¹² L. E. Piilonen,⁴⁸ M. Rozanska,²⁵ H. Sagawa,⁷
Y. Sakai,⁷ T. R. Sarangi,⁷ N. Sato,²⁰ T. Schietinger,¹⁶ O. Schneider,¹⁶ P. Schönmeier,⁴²
J. Schümann,²⁴ C. Schwanda,¹⁰ A. J. Schwartz,⁴ K. Senyo,²⁰ M. E. Sevier,¹⁹ H. Shibuya,⁴⁰
B. Shwartz,¹ V. Sidorov,¹ A. Somov,⁴ N. Soni,³¹ R. Stamen,⁷ S. Stanič,²⁸ M. Starič,¹²
K. Sumisawa,³⁰ T. Sumiyoshi,⁴⁵ S. Suzuki,³⁴ S. Y. Suzuki,⁷ F. Takasaki,⁷ N. Tamura,²⁷
M. Tanaka,⁷ Y. Teramoto,²⁹ X. C. Tian,³² T. Tsuboyama,⁷ T. Tsukamoto,⁷
S. Uehara,⁷ T. Uglov,¹¹ K. Ueno,²⁴ S. Uno,⁷ P. Urquijo,¹⁹ Y. Ushiroda,⁷ G. Varner,⁶
K. E. Varvell,³⁸ S. Villa,¹⁶ C. C. Wang,²⁴ C. H. Wang,²³ M.-Z. Wang,²⁴ Y. Watanabe,⁴⁴
Q. L. Xie,⁹ B. D. Yabsley,⁴⁸ A. Yamaguchi,⁴² Y. Yamashita,²⁶ M. Yamauchi,⁷
Heyoung Yang,³⁶ J. Zhang,⁷ L. M. Zhang,³⁵ Z. P. Zhang,³⁵ V. Zhilich,¹ and D. Žontar^{17,12}

(The Belle Collaboration)

¹*Budker Institute of Nuclear Physics, Novosibirsk*

²*Chiba University, Chiba*

³*Chonnam National University, Kwangju*

⁴*University of Cincinnati, Cincinnati, Ohio 45221*

- ⁵*Gyeongsang National University, Chinju*
⁶*University of Hawaii, Honolulu, Hawaii 96822*
⁷*High Energy Accelerator Research Organization (KEK), Tsukuba*
⁸*Hiroshima Institute of Technology, Hiroshima*
⁹*Institute of High Energy Physics, Chinese Academy of Sciences, Beijing*
¹⁰*Institute of High Energy Physics, Vienna*
¹¹*Institute for Theoretical and Experimental Physics, Moscow*
¹²*J. Stefan Institute, Ljubljana*
¹³*Kanagawa University, Yokohama*
¹⁴*Korea University, Seoul*
¹⁵*Kyungpook National University, Taegu*
¹⁶*Swiss Federal Institute of Technology of Lausanne, EPFL, Lausanne*
¹⁷*University of Ljubljana, Ljubljana*
¹⁸*University of Maribor, Maribor*
¹⁹*University of Melbourne, Victoria*
²⁰*Nagoya University, Nagoya*
²¹*Nara Women's University, Nara*
²²*National Central University, Chung-li*
²³*National United University, Miao Li*
²⁴*Department of Physics, National Taiwan University, Taipei*
²⁵*H. Niewodniczanski Institute of Nuclear Physics, Krakow*
²⁶*Nippon Dental University, Niigata*
²⁷*Niigata University, Niigata*
²⁸*Nova Gorica Polytechnic, Nova Gorica*
²⁹*Osaka City University, Osaka*
³⁰*Osaka University, Osaka*
³¹*Panjab University, Chandigarh*
³²*Peking University, Beijing*
³³*Princeton University, Princeton, New Jersey 08544*
³⁴*Saga University, Saga*
³⁵*University of Science and Technology of China, Hefei*
³⁶*Seoul National University, Seoul*
³⁷*Sungkyunkwan University, Suwon*
³⁸*University of Sydney, Sydney NSW*
³⁹*Tata Institute of Fundamental Research, Bombay*
⁴⁰*Toho University, Funabashi*
⁴¹*Tohoku Gakuin University, Tagajo*
⁴²*Tohoku University, Sendai*
⁴³*Department of Physics, University of Tokyo, Tokyo*
⁴⁴*Tokyo Institute of Technology, Tokyo*
⁴⁵*Tokyo Metropolitan University, Tokyo*
⁴⁶*Tokyo University of Agriculture and Technology, Tokyo*
⁴⁷*University of Tsukuba, Tsukuba*
⁴⁸*Virginia Polytechnic Institute and State University, Blacksburg, Virginia 24061*
⁴⁹*Yonsei University, Seoul*

(Dated: June 29, 2018)

Abstract

We present new measurements of CP -violation parameters in $B^0 \rightarrow \phi K^0$, $K^+ K^- K_S^0$, $f_0(980) K_S^0$, $\eta' K_S^0$, ωK_S^0 , and $K_S^0 \pi^0$ decays based on a sample of 275×10^6 $B\bar{B}$ pairs collected at the $\Upsilon(4S)$ resonance with the Belle detector at the KEKB energy-asymmetric e^+e^- collider. One neutral B meson is fully reconstructed in one of the specified decay channels, and the flavor of the accompanying B meson is identified from its decay products. CP -violation parameters for each of the decay modes are obtained from the asymmetries in the distributions of the proper-time intervals between the two B decays. The combined result for the $B^0 \rightarrow \phi K^0$, $K^+ K^- K_S^0$, $f_0(980) K_S^0$, $\eta' K_S^0$, ωK_S^0 , $K_S^0 \pi^0$ and previously reported $K_S^0 K_S^0 K_S^0$ decays differs from the SM expectation by 2.4 standard deviations.

PACS numbers: 11.30.Er, 12.15.Hh, 13.25.Hw

I. INTRODUCTION

The flavor-changing $b \rightarrow s$ transition proceeds through loop penguin diagrams. Such loop diagrams play an important role in testing the standard model (SM) and new physics because particles beyond the SM can contribute via additional loop diagrams. CP violation in the $b \rightarrow s$ transition is especially sensitive to physics at a very high-energy scale [1]. Theoretical studies indicate that large deviations from the SM expectations are allowed for time-dependent CP asymmetries in B^0 meson decays [2]. Experimental investigations have recently been launched at the two B factories, each of which has produced more than 10^8 $B\bar{B}$ pairs. Our previous measurement of the CP -violating asymmetry in $B^0 \rightarrow \phi K_S^0$ [3], which is dominated by the $b \rightarrow s\bar{s}s$ transition, yielded a value that differs from the SM expectation by 3.5 standard deviations [4]. Measurements with a larger data sample are required to elucidate this difference. It is also essential to examine additional modes that may be sensitive to the same $b \rightarrow s$ penguin amplitude. In this spirit, experimental results using the decay modes $B^0 \rightarrow \phi K_L^0$, $K^+K^-K_S^0$, $f_0(980)K_S^0$, $\eta'K_S^0$, and $K_S^0\pi^0$ have already been reported [4, 5].

In the SM, CP violation arises from a single irreducible phase, the Kobayashi-Maskawa (KM) phase [6], in the weak-interaction quark-mixing matrix. In particular, the SM predicts CP asymmetries in the time-dependent rates for B^0 and \bar{B}^0 decays to a common CP eigenstate f_{CP} [7]. In the decay chain $\Upsilon(4S) \rightarrow B^0\bar{B}^0 \rightarrow f_{CP}f_{\text{tag}}$, where one of the B mesons decays at time t_{CP} to a final state f_{CP} and the other decays at time t_{tag} to a final state f_{tag} that distinguishes between B^0 and \bar{B}^0 , the decay rate has a time dependence given by

$$\mathcal{P}(\Delta t) = \frac{e^{-|\Delta t|/\tau_{B^0}}}{4\tau_{B^0}} \left\{ 1 + q \cdot [\mathcal{S} \sin(\Delta m_d \Delta t) + \mathcal{A} \cos(\Delta m_d \Delta t)] \right\}. \quad (1)$$

Here \mathcal{S} and \mathcal{A} are CP -violation parameters, τ_{B^0} is the B^0 lifetime, Δm_d is the mass difference between the two B^0 mass eigenstates, $\Delta t = t_{CP} - t_{\text{tag}}$, and the b -flavor charge $q = +1$ (-1) when the tagging B meson is a B^0 (\bar{B}^0). To a good approximation, the SM predicts $\mathcal{S} = -\xi_f \sin 2\phi_1$, where $\xi_f = +1(-1)$ corresponds to CP -even (-odd) final states, and $\mathcal{A} = 0$ for both $b \rightarrow c\bar{c}s$ and $b \rightarrow s\bar{q}q$ transitions. Recent measurements of time-dependent CP asymmetries in $B^0 \rightarrow J/\psi K_S^0$ and related decay modes by Belle [8, 9] and BaBar [10], which are governed by the $b \rightarrow c\bar{c}s$ transition, have already determined $\sin 2\phi_1$ rather precisely; the present world average value is $\sin 2\phi_1 = +0.726 \pm 0.037$ [11]. This serves as a firm reference point for the SM.

Belle's previous measurements for $B^0 \rightarrow \phi K_S^0$, $K^+K^-K_S^0$ and $\eta'K_S^0$ were based on a 140 fb^{-1} data sample (DS-I) containing 152×10^6 $B\bar{B}$ pairs. In this report, we describe improved measurements incorporating an additional 113 fb^{-1} data sample that contains 123×10^6 $B\bar{B}$ pairs (DS-II) for a total of 275×10^6 $B\bar{B}$ pairs.

While ϕK_S^0 and $\eta'K_S^0$ final states are CP eigenstates with $\xi_f = -1$, the $K^+K^-K_S^0$ final state is in general a mixture of both $\xi_f = +1$ and -1 . Excluding K^+K^- pairs that are consistent with a $\phi \rightarrow K^+K^-$ decay from the $B^0 \rightarrow K^+K^-K_S^0$ sample, we find that the $K^+K^-K_S^0$ state is primarily $\xi_f = +1$; a measurement of the $\xi_f = +1$ fraction using the isospin relation [12] with a 253 fb^{-1} data sample gives $f_+ = 0.83 \pm 0.10(\text{stat}) \pm 0.04(\text{syst})$, which is consistent with the previous result [4]. The SM expectation for this mode is $\mathcal{S} = -(2f_+ - 1) \sin 2\phi_1$.

We include additional ϕK_S^0 and $\eta'K_S^0$ subdecay modes that were not used in the previous analysis. We also describe new measurements of CP asymmetries for the following CP -eigenstate B^0 decay modes: $B^0 \rightarrow \phi K_L^0$ and $f_0(980)K_S^0$ for $\xi_f = +1$; $B^0 \rightarrow \omega K_S^0$ and $K_S^0\pi^0$

for $\xi_f = -1$. The decays $B^0 \rightarrow \phi K_S^0$ and ϕK_L^0 are combined in this analysis by redefining \mathcal{S} as $-\xi_f \mathcal{S}$ to take the opposite CP eigenvalues into account, and are collectively called “ $B^0 \rightarrow \phi K^0$ ”. The CP asymmetries for the decay $B^0 \rightarrow \omega K_S^0$ are measured for the first time.

At the KEKB energy-asymmetric e^+e^- (3.5 on 8.0 GeV) collider [13], the $\Upsilon(4S)$ is produced with a Lorentz boost of $\beta\gamma = 0.425$ nearly along the electron beamline (z). Since the B^0 and \bar{B}^0 mesons are approximately at rest in the $\Upsilon(4S)$ center-of-mass system (cms), Δt can be determined from the displacement in z between the f_{CP} and f_{tag} decay vertices: $\Delta t \simeq (z_{CP} - z_{\text{tag}})/(\beta\gamma c) \equiv \Delta z/(\beta\gamma c)$.

The Belle detector is a large-solid-angle magnetic spectrometer that consists of a silicon vertex detector (SVD), a 50-layer central drift chamber (CDC), an array of aerogel threshold Cherenkov counters (ACC), a barrel-like arrangement of time-of-flight scintillation counters (TOF), and an electromagnetic calorimeter comprised of CsI(Tl) crystals (ECL) located inside a superconducting solenoid coil that provides a 1.5 T magnetic field. An iron flux-return located outside of the coil is instrumented to detect K_L^0 mesons and to identify muons (KLM). The detector is described in detail elsewhere [14]. Two inner detector configurations were used. A 2.0 cm radius beampipe and a 3-layer silicon vertex detector (SVD-I) were used for DS-I, while a 1.5 cm radius beampipe, a 4-layer silicon detector (SVD-II) and a small-cell inner drift chamber were used for DS-II [15].

II. EVENT SELECTION, FLAVOR TAGGING AND VERTEX RECONSTRUCTION

A. Overview

We reconstruct the following B^0 decay modes to measure CP asymmetries: $B^0 \rightarrow \phi K_S^0$, ϕK_L^0 , $K^+K^-K_S^0$, $f_0(980)K_S^0$, $\eta'K_S^0$, ωK_S^0 , and $K_S^0\pi^0$. We exclude K^+K^- pairs that are consistent with a $\phi \rightarrow K^+K^-$ decay from the $B^0 \rightarrow K^+K^-K_S^0$ sample. The intermediate meson states are reconstructed from the following decays: $\pi^0 \rightarrow \gamma\gamma$, $K_S^0 \rightarrow \pi^+\pi^-$ (also $\pi^0\pi^0$ for the ϕK_S^0 decay), $\eta \rightarrow \gamma\gamma$ or $\pi^+\pi^-\pi^0$, $\rho^0 \rightarrow \pi^+\pi^-$, $\omega \rightarrow \pi^+\pi^-\pi^0$, $\eta' \rightarrow \rho^0\gamma$ or $\eta\pi^+\pi^-$, $f_0(980) \rightarrow \pi^+\pi^-$, and $\phi \rightarrow K^+K^-$.

Among the decay chains listed above, $B^0 \rightarrow \phi K_S^0$ ($K_S^0 \rightarrow \pi^+\pi^-$), $B^0 \rightarrow K^+K^-K_S^0$, $B^0 \rightarrow \eta'K_S^0$ ($\eta' \rightarrow \rho^0\gamma$), and $B^0 \rightarrow \eta'K_S^0$ ($\eta' \rightarrow \eta\pi^+\pi^-$, $\eta \rightarrow \gamma\gamma$) decays were used in the previous analysis [4]. The selection criteria for these decays remain the same. For the newly included B^0 decay modes, identification of photons, neutral and charged kaons, and neutral and charged pions is based on the procedure used previously. However, the selection criteria for each B^0 decay mode were optimized individually and are thus different from one another.

B. $B^0 \rightarrow \phi K_S^0$ and $K^+K^-K_S^0$

Charged tracks reconstructed with the CDC for kaon and pion candidates except for those from $K_S^0 \rightarrow \pi^+\pi^-$ decays are required to originate from the interaction point (IP). We distinguish charged kaons from pions based on a kaon (pion) likelihood $\mathcal{L}_{K(\pi)}$ derived from the TOF, ACC and dE/dx measurements in the CDC.

Pairs of oppositely charged tracks that have an invariant mass within $0.030 \text{ GeV}/c^2$ of the nominal K_S^0 mass are used to reconstruct $K_S^0 \rightarrow \pi^+\pi^-$ decays. The distance of closest

approach of the candidate charged tracks to the IP in the plane perpendicular to z axis is required to be larger than 0.02 cm for high momentum (> 1.5 GeV/ c) K_S^0 candidates and 0.03 cm for those with momentum less than 1.5 GeV/ c . The $\pi^+\pi^-$ vertex is required to be displaced from the IP by a minimum transverse distance of 0.22 cm for high-momentum candidates and 0.08 cm for the remaining candidates. The mismatch in the z direction at the K_S^0 vertex point for the $\pi^+\pi^-$ tracks must be less than 2.4 cm for high-momentum candidates and 1.8 cm for the remaining candidates. The direction of the pion pair momentum must also agree with the direction of the vertex point from the IP to within 0.03 rad for high-momentum candidates, and to within 0.1 rad for the remaining candidates. The resolution of the reconstructed K_S^0 mass is 0.003 GeV/ c^2 .

Photons are identified as isolated ECL clusters that are not matched to any charged track. To select $K_S^0 \rightarrow \pi^0\pi^0$ decays, we reconstruct π^0 candidates from pairs of photons with $E_\gamma > 0.05$ GeV, where E_γ is the photon energy measured with the ECL. Photon pairs with an invariant mass between 0.08 and 0.15 GeV/ c^2 and a momentum above 0.1 GeV/ c are used as π^0 candidates. Initially, the π^0 decay vertex is assumed to be the IP. The asymmetric mass window is used to take into account the lower tail of the mass distribution due to the distance between the IP and the true π^0 vertex. Candidate $K_S^0 \rightarrow \pi^0\pi^0$ decays are required to have an invariant mass between 0.47 GeV/ c^2 and 0.52 GeV/ c^2 , where we perform a fit with constraints on the K_S^0 vertex and the π^0 masses to improve the $\pi^0\pi^0$ invariant mass resolution. We also require that the distance between the IP and the reconstructed K_S^0 decay vertex be larger than -10 cm, where the positive direction is defined by the K_S^0 momentum.

Candidate $\phi \rightarrow K^+K^-$ decays are required to have an invariant mass that is within 0.01 GeV/ c^2 of the nominal ϕ meson mass. Since the ϕ meson selection is effective in reducing background events, we impose only minimal kaon-identification requirements; $\mathcal{R}_{K/\pi} \equiv \mathcal{L}_K/(\mathcal{L}_K + \mathcal{L}_\pi) > 0.1$ is required, where the kaon likelihood ratio $\mathcal{R}_{K/\pi}$ has values between 0 (likely to be a pion) and 1 (likely to be a kaon). We use a more stringent kaon-identification requirement, $\mathcal{R}_{K/\pi} > 0.6$, to select non-resonant K^+K^- candidates for the decay $B^0 \rightarrow K^+K^-K_S^0$. The K^+K^- candidates for $B^0 \rightarrow K^+K^-K_S^0$ are selected by rejecting K^+K^- pairs with an invariant mass within 0.015 GeV/ c^2 of the nominal ϕ meson mass, reducing the ϕ contribution to a negligible level. To remove $\chi_{c0} \rightarrow K^+K^-$, $J/\psi \rightarrow K^+K^-$ and $D^0 \rightarrow K^+K^-$ decays, K^+K^- pairs with an invariant mass within 0.015 GeV/ c^2 of the nominal masses of χ_{c0} and J/ψ or within 0.01 GeV/ c^2 of the nominal D^0 mass are rejected. $D^+ \rightarrow K_S^0K^+$ decays are also removed by rejecting $K_S^0K^+$ pairs with an invariant mass within 0.01 GeV/ c^2 of the nominal D^+ mass.

For reconstructed $B \rightarrow f_{CP}$ candidates, we identify B meson decays using the energy difference $\Delta E \equiv E_B^{\text{cms}} - E_{\text{beam}}^{\text{cms}}$ and the beam-energy constrained mass $M_{\text{bc}} \equiv \sqrt{(E_{\text{beam}}^{\text{cms}})^2 - (p_B^{\text{cms}})^2}$, where $E_{\text{beam}}^{\text{cms}}$ is the beam energy in the cms, and E_B^{cms} and p_B^{cms} are the cms energy and momentum of the reconstructed B candidate, respectively. The resolution of M_{bc} is about 0.003 GeV/ c^2 . Because of the smallness of p_B^{cms} , the M_{bc} resolution is dominated by the beam-energy spread which is common to all decay modes. The resolution of ΔE depends on the reconstructed decay mode. The ΔE resolution is 0.013 GeV for ϕK_S^0 ($K_S^0 \rightarrow \pi^+\pi^-$) and $K^+K^-K_S^0$. The ΔE distribution for ϕK_S^0 ($K_S^0 \rightarrow \pi^0\pi^0$) has a tail toward lower ΔE due to γ energy leaking in the ECL. The ΔE resolution for ϕK_S^0 ($K_S^0 \rightarrow \pi^0\pi^0$) is 0.058 GeV for the main component and the width of the tail component is about 0.14 GeV. The B meson signal region is defined as $|\Delta E| < 0.06$ GeV for $B^0 \rightarrow \phi K_S^0$ ($K_S^0 \rightarrow \pi^+\pi^-$), -0.15 GeV $< \Delta E < 0.1$ GeV for $B^0 \rightarrow \phi K_S^0$ ($K_S^0 \rightarrow \pi^0\pi^0$), $|\Delta E| < 0.04$ GeV for $B^0 \rightarrow K^+K^-K_S^0$, and 5.27 GeV/ $c^2 < M_{\text{bc}} < 5.29$ GeV/ c^2 for all

decays.

The dominant background to the $B^0 \rightarrow \phi K_S^0$ decay comes from $e^+e^- \rightarrow u\bar{u}$, $d\bar{d}$, $s\bar{s}$, or $c\bar{c}$ continuum events. Since these tend to be jet-like, while the signal events tend to be spherical, we use a set of variables that characterize the event topology to distinguish between the two. We combine S_\perp , θ_T and modified Fox-Wolfram moments [16] into a Fisher discriminant \mathcal{F} , where S_\perp is the scalar sum of the transverse momenta of particles other than the reconstructed B candidate outside a 45° cone around the candidate ϕ meson direction (the thrust axis of the B candidate for $K^+K^-K_S^0$ decays) divided by the scalar sum of their total momenta, and θ_T is the angle between the thrust axis of the B candidate and that of the other particles in the cms. We also use the angle of the reconstructed B candidate with respect to the beam direction in the cms (θ_B), and the helicity angle θ_H defined as the angle between the B meson momentum and the daughter K^+ momentum in the ϕ meson rest frame. We combine \mathcal{F} , $\cos\theta_B$ and $\cos\theta_H$ into a signal [background] likelihood variable, which is defined as $\mathcal{L}_{\text{sig[bkg]}} \equiv \mathcal{L}_{\text{sig[bkg]}}(\mathcal{F}) \times \mathcal{L}_{\text{sig[bkg]}}(\cos\theta_B) \times \mathcal{L}_{\text{sig[bkg]}}(\cos\theta_H)$. For $K^+K^-K_S^0$ decays, \mathcal{F} and $\cos\theta_B$ are combined to make the likelihood variables. We impose requirements on the likelihood ratio $\mathcal{R}_{\text{s/b}} \equiv \mathcal{L}_{\text{sig}}/(\mathcal{L}_{\text{sig}} + \mathcal{L}_{\text{bkg}})$ to maximize the figure-of-merit (FoM) defined as $N_{\text{sig}}^{\text{MC}}/\sqrt{N_{\text{sig}}^{\text{MC}} + N_{\text{bkg}}}$, where $N_{\text{sig}}^{\text{MC}}$ (N_{bkg}) represents the expected number of signal (background) events in the signal region. We estimate $N_{\text{sig}}^{\text{MC}}$ using Monte Carlo (MC) events, while N_{bkg} is determined from events outside the signal region. The requirement for $\mathcal{R}_{\text{s/b}}$ depends both on the decay mode and on the flavor-tagging quality, r , which is described in Sec. II H. The threshold values range from 0.1 (used for $r > 0.875$) to 0.4 (used for $r < 0.25$) for the decay $B^0 \rightarrow \phi K_S^0$ ($K_S^0 \rightarrow \pi^+\pi^-$), and from 0.25 to 0.65 for the decay $B^0 \rightarrow K^+K^-K_S^0$. For the $B^0 \rightarrow K^+K^-K_S^0$ candidates, we also require $|\cos\theta_T| < 0.9$ prior to the $\mathcal{R}_{\text{s/b}}$ requirement. We impose a more stringent requirement, $\mathcal{R}_{\text{s/b}} > 0.75$, for all r values in the decay $B^0 \rightarrow \phi K_S^0$ ($K_S^0 \rightarrow \pi^0\pi^0$). The $\mathcal{R}_{\text{s/b}}$ requirement reduces the continuum background by 73% for $B^0 \rightarrow \phi K_S^0$ ($K_S^0 \rightarrow \pi^+\pi^-$), 92% for $B^0 \rightarrow K^+K^-K_S^0$ and 94% for $B^0 \rightarrow \phi K_S^0$ ($K_S^0 \rightarrow \pi^0\pi^0$), retaining 91% of the signal for $B^0 \rightarrow \phi K_S^0$ ($K_S^0 \rightarrow \pi^+\pi^-$), 72% for $B^0 \rightarrow K^+K^-K_S^0$ and 71% for $B^0 \rightarrow \phi K_S^0$ ($K_S^0 \rightarrow \pi^0\pi^0$).

We use events outside the signal region as well as a large MC sample to study the background components. The dominant background is from continuum. The contributions from $B\bar{B}$ events are small. We estimate the contamination of $B^0 \rightarrow K^+K^-K_S^0$ and $B^0 \rightarrow f_0(980)K_S^0$ ($f_0(980) \rightarrow K^+K^-$) decays in the $B^0 \rightarrow \phi K_S^0$ sample from the B yields in K^+K^- mass sideband data. The contamination of $B^0 \rightarrow K^+K^-K_S^0$ events in the $B^0 \rightarrow \phi K_S^0$ sample is $7.1 \pm 1.6\%$ ($6.2 \pm 2.0\%$) for DS-I (DS-II). Backgrounds from the decay $B^0 \rightarrow f_0(980)K_S^0$ ($f_0(980) \rightarrow K^+K^-$), which has a CP eigenvalue opposite to ϕK_S^0 , are found to be $0.4^{+1.9}_{-0.4}\%$ ($0.0^{+2.0}_{-0.0}\%$) for DS-I (DS-II). The influence of these backgrounds is treated as a source of systematic uncertainty.

Figures 1(a) and (c) show the M_{bc} distributions for the reconstructed $B^0 \rightarrow \phi K_S^0$ and $K^+K^-K_S^0$ candidates within the ΔE signal regions after flavor tagging and vertex reconstruction. The ΔE distributions for the $B^0 \rightarrow \phi K_S^0$ and $K^+K^-K_S^0$ candidates within the M_{bc} signal region are shown in Fig. 2(a) and (b), respectively. The signal yield is determined from an unbinned two-dimensional maximum-likelihood fit to the ΔE - M_{bc} distribution in the fit region defined as $M_{\text{bc}} > 5.2 \text{ GeV}/c^2$ for all modes, and $-0.12 \text{ GeV} < \Delta E < 0.25 \text{ GeV}$ for the $B^0 \rightarrow \phi K_S^0$ ($K_S^0 \rightarrow \pi^+\pi^-$) or $K^+K^-K_S^0$ decay and $-0.15 \text{ GeV} < \Delta E < 0.25 \text{ GeV}$ for the $B^0 \rightarrow \phi K_S^0$ ($K_S^0 \rightarrow \pi^0\pi^0$) decay. The ϕK_S^0 ($K_S^0 \rightarrow \pi^+\pi^-$) signal distribution is modeled with a Gaussian function (a sum of two Gaussian functions) for M_{bc} (ΔE). The ϕK_S^0 ($K_S^0 \rightarrow \pi^0\pi^0$) signal distribution is modeled with a smoothed histogram obtained from

MC events. For the continuum background, we use the ARGUS parameterization [17] for M_{bc} and a linear function for ΔE . The fits yield 139 ± 14 $B^0 \rightarrow \phi K_S^0$ events and 398 ± 28 $B^0 \rightarrow K^+ K^- K_S^0$ events in the signal region, where the errors are statistical only.

C. $B^0 \rightarrow \phi K_L^0$

Candidate $\phi \rightarrow K^+ K^-$ decays are selected with the criteria described above. We select K_L^0 candidates based on KLM and ECL information. There are two classes of K_L^0 candidates, which we refer to as KLM and ECL candidates. The requirements for the KLM candidates are the same as those used in the $B^0 \rightarrow J/\psi K_L^0$ selection for the $\sin 2\phi_1$ measurement [8]. ECL candidates are selected from ECL clusters using a K_L^0 likelihood ratio [8], which is calculated from the following information: the distance between the ECL cluster and the closest extrapolated charged track position; the ECL cluster energy; E_9/E_{25} , the ratio of energies summed in 3×3 and 5×5 arrays of CsI(Tl) crystals surrounding the crystal at the center of the shower; the ECL shower width and the invariant mass of the shower. The likelihood ratio is required to be greater than 0.8. For both KLM and ECL candidates, we also require that the cosine of the angle between the K_L^0 direction and the direction of the missing momentum of the event in the laboratory frame be greater than 0.6.

Since the energy of the K_L^0 is not measured, M_{bc} and ΔE cannot be calculated in the same way that is used for the other final states. Using the four-momentum of a reconstructed ϕ candidate and the K_L^0 flight direction, we calculate the momentum of the K_L^0 candidate requiring $\Delta E = 0$. We then calculate p_B^{cms} , the momentum of the B candidate in the cms, and define the B meson signal region as $0.2 \text{ GeV}/c < p_B^{\text{cms}} < 0.5 \text{ GeV}/c$. We impose the requirement $\mathcal{R}_{s/b} > 0.98$ to reduce the continuum background by 99.4%. The signal efficiency of the $\mathcal{R}_{s/b}$ requirement is 28.1%. Here $\mathcal{R}_{s/b}$ is based on the discriminating variables used for the $B^0 \rightarrow \phi K_S^0$ decay and the number of tracks originating from the IP with a momentum above $0.1 \text{ GeV}/c$. The $\mathcal{R}_{s/b}$ requirement is chosen to optimize the FoM, which is calculated taking the background from both continuum and generic B decays into account. The K_L^0 detection efficiency difference between data and MC is studied using the decay $B^0 \rightarrow J/\psi K_L^0$, and corrections are applied to the $B^0 \rightarrow \phi K_L^0$ MC events to calculate the FoM. If there is more than one candidate $B^0 \rightarrow \phi K_L^0$ decay in the signal region, we take the one with the highest $\mathcal{R}_{s/b}$ value. ECL candidates are not used if there is a candidate $B^0 \rightarrow \phi K_L^0$ decay with a KLM candidate. We find that about 90% of signal events are reconstructed with KLM candidates.

We study the background components using a large MC sample as well as data taken with cms energy 60 MeV below the nominal $\Upsilon(4S)$ mass (off-resonance data). The dominant background is from continuum. A MC study with the efficiency correction obtained from $B^0 \rightarrow J/\psi K_L^0$ data yields 9 ± 5 background events from B decays, which include $B^0 \rightarrow \phi K^{*0}$, ϕK_S^0 and $B^+ \rightarrow \phi K^{*+}$ decays. The influence of these backgrounds, including their CP asymmetries, is treated as a source of systematic uncertainty.

The p_B^{cms} distribution after flavor tagging and vertex reconstruction is shown in Fig. 1(b). The signal yield is determined from an extended unbinned maximum-likelihood fit in the range $p_B^{\text{cms}} < 1 \text{ GeV}/c$. The $B^0 \rightarrow \phi K_L^0$ signal shape is obtained from MC events. Background from $B\bar{B}$ pairs is also modeled with MC. We fix the ratio between the signal yield and the $B\bar{B}$ background based on known branching fractions and reconstruction efficiencies; the uncertainty in the ratio is treated as a source of systematic error. The continuum background distribution is represented by a smoothed histogram obtained from MC events; we

confirm that the function describes the off-resonance data well. The fit yields $36 \pm 15 \pm 10$ $B^0 \rightarrow \phi K_L^0$ events, where the first error is statistical and the second error is systematic. The sources of the systematic error include uncertainties in the efficiency corrections, in $B\bar{B}$ background branching fractions and in the background parameterizations. The result is in good agreement with the expected $B^0 \rightarrow \phi K_L^0$ signal yield (36 ± 9 events) obtained from MC after applying the efficiency correction from the $B^0 \rightarrow J/\psi K_L^0$ data.

D. $B^0 \rightarrow f_0(980)K_S^0$

Candidate $K_S^0 \rightarrow \pi^+\pi^-$ decays are selected with criteria that are slightly different from those used for the $B^0 \rightarrow \phi K_S^0$ decay so as to obtain the best performance for the $B^0 \rightarrow f_0(980)K_S^0$ decay. Pairs of oppositely charged pions that have invariant masses between 0.890 and 1.088 GeV/c^2 are used to reconstruct $f_0(980) \rightarrow \pi^+\pi^-$ decays. Tracks that are identified as kaons ($\mathcal{R}_{K/\pi} > 0.7$) or electrons are not used. We require that both $K_S^0\pi^+$ and $K_S^0\pi^-$ combinations have invariant masses more than 0.1 GeV/c^2 above the nominal charged D meson mass; this removes background from $D^\pm \rightarrow K_S^0\pi^\pm$ and $K^{*\pm} \rightarrow K_S^0\pi^\pm$ decays.

The B meson signal region is defined as $|\Delta E| < 0.06 \text{ GeV}$ and $5.27 \text{ GeV}/c^2 < M_{bc} < 5.29 \text{ GeV}/c^2$. The ΔE resolution is 0.019 GeV . The dominant background is from continuum. For the continuum suppression, we require $\mathcal{R}_{s/b} > 0.6$ for events with the best-quality flavor tagging ($r > 0.875$), and $\mathcal{R}_{s/b} > 0.8$ for other events. The continuum background is reduced by 95%, retaining 60% of signal events. Here the signal likelihood ratio $\mathcal{R}_{s/b}$ is obtained from $\cos\theta_B$ and \mathcal{F} , which consists of the modified Fox-Wolfram moments and $\cos\theta_T$.

Figure 1(d) shows the M_{bc} distribution for the reconstructed $B^0 \rightarrow f_0(980)K_S^0$ candidates within the ΔE signal region after flavor tagging and vertex reconstruction. The ΔE distribution for the $B^0 \rightarrow f_0(980)K_S^0$ candidates within the M_{bc} signal region is shown in Fig. 2(c). For the signal yield extraction, we first perform an unbinned two-dimensional maximum-likelihood fit to the ΔE - M_{bc} distribution in the fit region defined as $M_{bc} > 5.2 \text{ GeV}/c^2$ and $-0.3 \text{ GeV} < \Delta E < 0.4 \text{ GeV}$. The signal is modeled with a Gaussian function (a sum of two Gaussian functions) for M_{bc} (ΔE). For the continuum background, we use the ARGUS parameterization for M_{bc} and a linear function for ΔE . The fit yields the number of $B^0 \rightarrow \pi^+\pi^-K_S^0$ events that have $\pi^+\pi^-$ invariant masses within the $f_0(980)$ resonance region, which may include contributions from $B^0 \rightarrow \rho^0 K_S^0$ as well as non-resonant three-body $B^0 \rightarrow \pi^+\pi^-K_S^0$ decays. To separate these peaking backgrounds from the $B^0 \rightarrow f_0(980)K_S^0$ decay, we perform another fit to the $\pi^+\pi^-$ invariant mass distribution for the events inside the ΔE - M_{bc} signal region. We use Breit-Wigner functions for the $B^0 \rightarrow f_0(980)K_S^0$ signal as well as for $B^0 \rightarrow \rho K_S^0$ and a possible resonance above the $f_0(980)$ mass region, which is referred to as $f_X(1300)$. We use the masses and widths of $f_0(980)$ and $f_X(1300)$ obtained from data [12]. Three-body $B^0 \rightarrow \pi^+\pi^-K_S^0$ decays are modeled with a fourth-order polynomial function. The continuum background is modeled with a sum of a threshold function and a Breit-Wigner function for ρ resonance. The $\pi^+\pi^-$ invariant mass distribution with the fit result is shown in Fig. 3. The fit yields 94 ± 14 $B^0 \rightarrow f_0(980)K_S^0$ events. The peaking background contribution in the ΔE - M_{bc} signal region is estimated to be 9 ± 3 events.

E. $B^0 \rightarrow \eta' K_S^0$

Candidate $K_S^0 \rightarrow \pi^+\pi^-$ decays are selected with the same criteria as those used for the $B^0 \rightarrow \phi K_S^0$ decay. Charged pions from the η , ρ^0 or η' decay are selected from tracks originating from the IP. We reject kaon candidates by requiring $\mathcal{R}_{K/\pi} < 0.9$. Candidate photons from $\pi^0 \rightarrow \gamma\gamma$ decays are required to have $E_\gamma > 0.05$ GeV. The reconstructed π^0 candidate is required to satisfy $0.118 \text{ GeV}/c^2 < M_{\gamma\gamma} < 0.15 \text{ GeV}/c^2$ and $p_{\pi^0}^{\text{cms}} > 0.1 \text{ GeV}/c$, where $M_{\gamma\gamma}$ and $p_{\pi^0}^{\text{cms}}$ are the invariant mass and the momentum in the cms, respectively. Candidate photons from $\eta \rightarrow \gamma\gamma$ ($\eta' \rightarrow \rho^0\gamma$) decays are required to have $E_\gamma > 0.05$ (0.1) GeV. The invariant mass of the photon pair is required to be between 0.5 and 0.57 GeV/c^2 for the $\eta \rightarrow \gamma\gamma$ decay. The $\pi^+\pi^-\pi^0$ invariant mass is required to be between 0.535 and 0.558 GeV/c^2 for the $\eta \rightarrow \pi^+\pi^-\pi^0$ decay. A kinematic fit with an η mass constraint is performed using the fitted vertex of the $\pi^+\pi^-$ tracks from the η' as the decay point. For $\eta' \rightarrow \rho^0\gamma$ decays, candidate ρ^0 mesons are reconstructed from pairs of vertex-constrained $\pi^+\pi^-$ tracks with an invariant mass between 0.55 and 0.92 GeV/c^2 . The $\eta' \rightarrow \eta\pi^+\pi^-$ candidates are required to have a reconstructed mass between 0.94 and 0.97 GeV/c^2 (0.95 and 0.966 GeV/c^2) for the $\eta \rightarrow \gamma\gamma$ ($\eta \rightarrow \pi^+\pi^-\pi^0$) decay. Candidate $\eta' \rightarrow \rho^0\gamma$ decays are required to have a reconstructed mass from 0.935 to 0.975 GeV/c^2 .

The B meson signal region is defined as $|\Delta E| < 0.06$ GeV for $B^0 \rightarrow \eta' K_S^0$ ($\eta' \rightarrow \rho^0\gamma$), $-0.1 \text{ GeV} < \Delta E < 0.08$ GeV for $B^0 \rightarrow \eta' K_S^0$ ($\eta' \rightarrow \eta\pi^+\pi^-$, $\eta \rightarrow \gamma\gamma$), $-0.08 \text{ GeV} < \Delta E < 0.06$ GeV for $B^0 \rightarrow \eta' K_S^0$ ($\eta' \rightarrow \eta\pi^+\pi^-$, $\eta \rightarrow \pi^+\pi^-\pi^0$), and $5.27 \text{ GeV}/c^2 < M_{\text{bc}} < 5.29 \text{ GeV}/c^2$ for all decays. The ΔE resolution is 0.017 GeV for $\eta' \rightarrow \rho^0\gamma$, 0.027 GeV for $\eta' \rightarrow \eta\pi^+\pi^-$ ($\eta \rightarrow \gamma\gamma$) and 0.018 GeV for $\eta' \rightarrow \eta\pi^+\pi^-$ ($\eta \rightarrow \pi^+\pi^-\pi^0$). The continuum suppression is based on the likelihood ratio $\mathcal{R}_{\text{s/b}}$ obtained from the same discriminating variables used for the $B^0 \rightarrow \phi K_S^0$ decay, except that we only use $\cos\theta_H$ for the decay $\eta' \rightarrow \rho\gamma$ ($\rho \rightarrow \pi^+\pi^-$), where θ_H is defined as the angle between the η' meson momentum and the daughter π^+ momentum in the ρ meson rest frame. The minimum $\mathcal{R}_{\text{s/b}}$ requirement depends both on the decay mode and on the flavor-tagging quality, and ranges from 0 (i.e., no requirement) to 0.4. For the $\eta' \rightarrow \rho^0\gamma$ mode, we also require $|\cos\theta_T| < 0.9$ prior to the $\mathcal{R}_{\text{s/b}}$ requirement. With these requirements, the continuum background is reduced by 87% for $\eta' \rightarrow \rho^0\gamma$, 58% for $\eta' \rightarrow \eta\pi^+\pi^-$ ($\eta \rightarrow \gamma\gamma$) and 31% for $\eta' \rightarrow \eta\pi^+\pi^-$ ($\eta \rightarrow \pi^+\pi^-\pi^0$), retaining 78% of the signal for $\eta' \rightarrow \rho^0\gamma$, 94% for $\eta' \rightarrow \eta\pi^+\pi^-$ ($\eta \rightarrow \gamma\gamma$) and 97% for $\eta' \rightarrow \eta\pi^+\pi^-$ ($\eta \rightarrow \pi^+\pi^-\pi^0$).

We use events outside the signal region as well as a large MC sample to study the background components. The dominant background is from continuum. In addition, according to MC simulation, there is a small ($\sim 3\%$) combinatorial background from $B\bar{B}$ events in $B^0 \rightarrow \eta' K_S^0$ ($\eta' \rightarrow \rho^0\gamma$). The contributions from $B\bar{B}$ events are smaller for other modes. The influence of these backgrounds is treated as a source of systematic uncertainty.

Figure 1(e) shows the M_{bc} distribution for the reconstructed $B^0 \rightarrow \eta' K_S^0$ candidates within the ΔE signal region after flavor tagging and vertex reconstruction, where all sub-decay modes are combined. The ΔE distribution for the $B^0 \rightarrow \eta' K_S^0$ candidates within the M_{bc} signal region is shown in Fig. 2(d). The signal yields are determined from unbinned two-dimensional maximum-likelihood fits to the ΔE - M_{bc} distributions in the fit region defined as $M_{\text{bc}} > 5.2 \text{ GeV}/c^2$ and $-0.25 \text{ GeV} < \Delta E < 0.25 \text{ GeV}$. We perform the fit for each final state separately. The $\eta' K_S^0$ signal distribution is modeled with a sum of two (three) Gaussian functions for M_{bc} (ΔE). For the continuum background, we use the ARGUS parameterization for M_{bc} and a linear function for ΔE . For the $\eta' \rightarrow \rho\gamma$ mode, we include the $B\bar{B}$ background shape obtained from MC in the fits. The fits yield a total of 512 ± 27

$B^0 \rightarrow \eta' K_S^0$ events in the signal region, where the error is statistical only.

F. $B^0 \rightarrow \omega K_S^0$

Candidate $K_S^0 \rightarrow \pi^+\pi^-$ decays are selected with criteria that are identical to those used for the $B^0 \rightarrow \phi K_S^0$ decay. Pions for the $\omega \rightarrow \pi^+\pi^-\pi^0$ decay are selected with the same criteria used for the $\eta \rightarrow \pi^+\pi^-\pi^0$ decay, except that we require $p_{\pi^0}^{\text{cms}} > 0.35 \text{ GeV}/c$. The $\pi^+\pi^-\pi^0$ invariant mass is required to be within $0.03 \text{ GeV}/c^2$ of the nominal ω mass. The B meson signal region is defined as $-0.10 \text{ GeV} < \Delta E < 0.08 \text{ GeV}$ and $5.27 \text{ GeV}/c^2 < M_{\text{bc}} < 5.29 \text{ GeV}/c^2$. The ΔE resolution is 0.028 GeV . The dominant background is from continuum. The continuum suppression is based on the likelihood ratio $\mathcal{R}_{\text{s/b}}$ obtained from the same discriminating variables used for the $B^0 \rightarrow \phi K_S^0$ decay; the helicity angle θ_H is defined as the angle between the B^0 meson momentum and the cross product of the π^+ and π^- momenta in the ω meson rest frame. We also require $|\cos \theta_T| < 0.9$ prior to the $\mathcal{R}_{\text{s/b}}$ requirement. The minimum $\mathcal{R}_{\text{s/b}}$ requirement depends on the flavor-tagging quality, and ranges from 0.3 (used for $r > 0.875$) to 0.9 (used for $r < 0.25$). The $\mathcal{R}_{\text{s/b}}$ and $|\cos \theta_T|$ requirements reject 98% of the continuum background while retaining 56% of the signal. The contribution from $B\bar{B}$ events is negligibly small.

Figure 1(f) shows the M_{bc} distribution for the reconstructed $B^0 \rightarrow \omega K_S^0$ candidates within the ΔE signal region after flavor tagging and vertex reconstruction. The ΔE distribution for the $B^0 \rightarrow \omega K_S^0$ candidates within the M_{bc} signal region is shown in Fig. 2(e). The signal yield is determined from an unbinned two-dimensional maximum-likelihood fit to the ΔE - M_{bc} distribution in the fit region defined as $M_{\text{bc}} > 5.2 \text{ GeV}/c^2$ and $-0.12 \text{ GeV} < \Delta E < 0.25 \text{ GeV}$. The signal distribution is modeled with a sum of two (three) Gaussian functions for M_{bc} (ΔE). For the continuum background, we use the ARGUS parameterization for M_{bc} and a linear function for ΔE . The fit yields 31 ± 7 $B^0 \rightarrow \omega K_S^0$ events in the signal region with a statistical significance (Σ) of 7.3, where Σ is defined as $\Sigma \equiv \sqrt{-2 \ln(\mathcal{L}_0/\mathcal{L}_{N_{\text{sig}}})}$, and \mathcal{L}_0 and $\mathcal{L}_{N_{\text{sig}}}$ denote the maximum likelihoods of the fits without and with the signal component, respectively.

G. $B^0 \rightarrow K_S^0 \pi^0$

Candidate $K_S^0 \rightarrow \pi^+\pi^-$ decays are selected with the same criteria as those used for the $B^0 \rightarrow \phi K_S^0$ decay, except that we impose a more stringent invariant mass requirement; only pairs of oppositely charged pions that have an invariant mass within $0.015 \text{ GeV}/c^2$ of the nominal K_S^0 mass are used. The π^0 selection criteria are the same as those used for the $B^0 \rightarrow \eta' K_S^0$ decay.

The B meson signal region is defined as $-0.15 \text{ GeV} < \Delta E < 0.1 \text{ GeV}$ and $5.27 \text{ GeV}/c^2 < M_{\text{bc}} < 5.29 \text{ GeV}/c^2$. The ΔE distribution for $K_S^0 \pi^0$ has a tail toward lower ΔE . The ΔE resolution is 0.047 GeV for the main component. The width of the tail is about 0.1 GeV . The dominant background is from continuum. In addition, according to MC simulation, there is a small ($\sim 2\%$) contamination from other charmless rare B decays. We use extended modified Fox-Wolfram moments, which were applied for the selection of the $B^0 \rightarrow \pi^0 \pi^0$ decay [18], to form a Fisher discriminant \mathcal{F} . We then combine likelihoods for \mathcal{F} and $\cos \theta_B$ to obtain the event likelihood ratio $\mathcal{R}_{\text{s/b}}$ for continuum suppression.

As described below, we include events that do not have B decay vertex information in our fit to obtain better sensitivity for the CP -violation parameter \mathcal{A} . For events with vertex information, the high- $\mathcal{R}_{s/b}$ region is defined as $\mathcal{R}_{s/b} > 0.78$ and the low- $\mathcal{R}_{s/b}$ region as $0.4 < \mathcal{R}_{s/b} \leq 0.78$. For events without vertex information, the high- $\mathcal{R}_{s/b}$ region is defined as $\mathcal{R}_{s/b} > 0.74$ (0.76) for DS-I (DS-II), and the low- $\mathcal{R}_{s/b}$ region as $0.4 < \mathcal{R}_{s/b} \leq 0.74$ (0.76) for DS-I (DS-II). By the high- $\mathcal{R}_{s/b}$ requirement, 95% of continuum backgrounds are rejected and 64% of signal events remain. As for the low- $\mathcal{R}_{s/b}$ region, 84% of continuum backgrounds are rejected and 26% of signal events remain.

Figure 1(g) shows the M_{bc} distribution for the high- $\mathcal{R}_{s/b}$ $B^0 \rightarrow K_S^0 \pi^0$ candidates within the ΔE signal region after flavor tagging and before vertex reconstruction. Also shown in Fig. 1(h) is the M_{bc} distribution for the low- $\mathcal{R}_{s/b}$ $B^0 \rightarrow K_S^0 \pi^0$ candidates. The ΔE distributions for the high- $\mathcal{R}_{s/b}$ and low- $\mathcal{R}_{s/b}$ candidates are shown in Fig. 2(f) and (g), respectively. The signal yield is determined from an unbinned two-dimensional maximum-likelihood fit to the ΔE - M_{bc} distribution in the fit region defined as $5.2 \text{ GeV}/c^2 < M_{bc} < 5.29 \text{ GeV}/c^2$ and $-0.5 \text{ GeV} < \Delta E < 0.5 \text{ GeV}$. The $B^0 \rightarrow K_S^0 \pi^0$ signal distribution is modeled with a Gaussian function for M_{bc} and with a Crystal Ball function [19] for ΔE . For the continuum background, we use the ARGUS parameterization for M_{bc} and a second-order Chebyshev function for ΔE . The B decay background distribution is represented by a smoothed histogram obtained from MC simulation. The fits yield 168 ± 16 and 79 ± 19 $B^0 \rightarrow K_S^0 \pi^0$ events in the high- $\mathcal{R}_{s/b}$ and low- $\mathcal{R}_{s/b}$ signal regions, respectively, where the errors are statistical only. The same procedure after the vertex reconstruction yields a total of 71 ± 13 $K_S^0 \pi^0$ events.

H. Flavor Tagging

The b -flavor of the accompanying B meson is identified from inclusive properties of particles that are not associated with the reconstructed $B^0 \rightarrow f_{CP}$ decay. We use the same procedure that is used for the $\sin 2\phi_1$ measurement [9]. The algorithm for flavor tagging is described in detail elsewhere [20]. We use two parameters, q and r , to represent the tagging information. The first, q , is defined in Eq. (1). The parameter r is an event-by-event, MC-determined flavor-tagging dilution factor that ranges from $r = 0$ for no flavor discrimination to $r = 1$ for unambiguous flavor assignment. It is used only to sort data into six r intervals listed in Table I. The wrong tag fractions for the six r intervals, w_l ($l = 1, 6$), and differences between B^0 and \bar{B}^0 decays, Δw_l , are determined from the data; we use the same values that were used for the $\sin 2\phi_1$ measurement [9] for DS-I. Wrong tag fractions for DS-II are separately obtained with the same procedure and are listed in Table I. The total effective tagging efficiency for DS-II is determined to be $\epsilon_{\text{eff}} \equiv \sum_{l=1}^6 \epsilon_l (1 - 2w_l)^2 = 0.30 \pm 0.01$, where ϵ_l is the event fraction for each r interval determined from the $J/\psi K_S^0$ data and is listed in Table I. The error includes both statistical and systematic uncertainties. We find that the wrong tag fractions for DS-II are slightly smaller than those for DS-I. As a result, the ϵ_{eff} value for DS-II is slightly larger than that for DS-I ($\epsilon_{\text{eff}} = 0.287 \pm 0.005$).

I. Vertex Reconstruction

The vertex position for the f_{CP} decay is reconstructed using charged tracks that have enough SVD hits; at least one layer with hits on both sides and at least one additional z

hit in other layers for SVD-I, and at least two layers with hits on both sides for SVD-II. A constraint on the IP is also used with the selected tracks; the IP profile is convolved with the finite B flight length in the plane perpendicular to the z axis. The pions from K_S^0 decays are not used except in the analysis of $B^0 \rightarrow K_S^0 \pi^0$ decays. The typical vertex reconstruction efficiency and z resolution for $B^0 \rightarrow \phi K_S^0$ decays are 95% and 78 μm , respectively. Similar values are obtained for other f_{CP} decays except for $B^0 \rightarrow K_S^0 \pi^0$ decays.

The vertex for $B^0 \rightarrow K_S^0 \pi^0$ decays is reconstructed using the K_S^0 trajectory and the IP constraint, where both pions from the K_S^0 decay are required to have enough SVD hits in the same way as that for other f_{CP} decays. The reconstruction efficiency depends both on the K_S^0 momentum and on the SVD geometry; the efficiency with SVD-II (32%) is higher than that with SVD-I (23%) because of the larger outer radius and the additional layer. The typical z resolution of the vertex reconstructed with the K_S^0 is 93 μm for SVD-I and 110 μm for SVD-II.

The f_{tag} vertex determination with SVD-I remains unchanged from the previous publication [4], and is described in detail elsewhere [21]; to minimize the effect of long-lived particles, secondary vertices from charmed hadrons and a small fraction of poorly reconstructed tracks, we adopt an iterative procedure in which the track that gives the largest contribution to the vertex χ^2 is removed at each step until a good χ^2 is obtained. The reconstruction efficiency was measured to be 93%. The typical z resolution is 140 μm [8].

For SVD-II, we find that the same vertex reconstruction algorithm results in a larger outlier fraction when only one track remains after the iteration procedure. Therefore, in this case, we repeat the iteration procedure with a more stringent requirement on the SVD-II hit pattern; at least two of the three outer layers have hits on both sides. The resulting outlier fraction, which is described in Sec. III, is comparable to that for SVD-I, while the inefficiency caused by this change is small (2.5%).

J. Summary of Signal Yields

The signal yields for $B^0 \rightarrow f_{CP}$ decays, N_{sig} , after flavor tagging and vertex reconstruction (before the vertex reconstruction for the decay $B^0 \rightarrow K_S^0 \pi^0$) are summarized in Table II. The signal purities are also listed in the table.

III. RESULTS OF CP ASYMMETRY MEASUREMENTS

We determine \mathcal{S} and \mathcal{A} for each mode by performing an unbinned maximum-likelihood fit to the observed Δt distribution. The probability density function (PDF) expected for the signal distribution, $\mathcal{P}_{\text{sig}}(\Delta t; \mathcal{S}, \mathcal{A}, q, w_l, \Delta w_l)$, is given by Eq. (1) incorporating the effect of incorrect flavor assignment. The distribution is convolved with the proper-time interval resolution function $R_{\text{sig}}(\Delta t)$, which takes into account the finite vertex resolution.

For the decays $B^0 \rightarrow \phi K_S^0$, $K^+ K^- K_S^0$, ϕK_L^0 , $f_0(980) K_S^0$, $\eta' K_S^0$ and ωK_S^0 , we use flavor-specific B decays governed by semileptonic or hadronic $b \rightarrow c$ transitions to determine the resolution function. We perform a simultaneous multiparameter fit to these high-statistics control samples to obtain the resolution function parameters, wrong-tag fractions (Section II H), Δm_d , τ_{B^+} and τ_{B^0} . We use the same resolution function used for the $\sin 2\phi_1$ measurement for DS-I [9]. For DS-II, the following modifications are introduced: a sum of two Gaussian functions is used to model the resolution of the f_{CP} vertex while a single

Gaussian function is used for DS-I; a sum of two Gaussian functions is used to model the resolution of the tag-side vertex obtained with one track and the IP constraint, while a single Gaussian function is used for DS-II. These modifications are needed to account for differences between SVD-I and SVD-II, as well as different background conditions in DS-I and DS-II. We test the new resolution parameterization using MC events on which we overlay beam-related background taken from data. A fit to the MC sample yields correct values for all parameters. With the multiparameter fit to data, we find that the standard deviation of the main Gaussian component of the resolution function is reduced from $78\ \mu\text{m}$ to $55\ \mu\text{m}$, which is consistent with our expectation from the improved impact parameter resolution of SVD-II [15]. The same fit also yields $\tau_{B^0} = 1.519 \pm 0.010\ \text{ps}$, $\tau_{B^+} = 1.652 \pm 0.012\ \text{ps}$ and $\Delta m_d = 0.516 \pm 0.007\ \text{ps}^{-1}$, where errors are statistical only. The results are consistent with those obtained with DS-I [9] and also with the world average values [22]. Thus we conclude that the resolution of SVD-II is well understood.

For the decay $B^0 \rightarrow K_S^0 \pi^0$, we use the resolution function described above with additional parameters that rescale vertex errors. The rescaling parameters depend on the detector configuration (SVD-I or SVD-II), SVD hit patterns of charged pions from the K_S^0 decay, and K_S^0 decay vertex position in the plane perpendicular to the beam axis. These parameters are determined from a fit to the Δt distribution of $B^0 \rightarrow J/\psi K_S^0$ data. Here the K_S^0 and the IP constraint are used for the vertex reconstruction, the B^0 lifetime is fixed at the world average value, and b -flavor tagging information is not used so that the expected PDF is an exponential function convolved with the resolution function.

We check the resulting resolution function by also reconstructing the vertex with leptons from J/ψ decays and the IP constraint. We find that the distribution of the distance between the vertex positions obtained with the two methods is well represented by the obtained resolution function convolved with the well-known resolution for the J/ψ vertex. Finally, we also perform a fit to the $B^0 \rightarrow J/\psi K_S^0$ sample with b -flavor information and obtain $\mathcal{S}_{J/\psi K_S^0} = +0.68 \pm 0.10(\text{stat})$ and $\mathcal{A}_{J/\psi K_S^0} = +0.02 \pm 0.04(\text{stat})$, which are in good agreement with the world average values. Thus, we conclude that the vertex resolution for the $B^0 \rightarrow K_S^0 \pi^0$ decay is well understood.

We determine the following likelihood value for each event:

$$\begin{aligned}
P_i = & (1 - f_{\text{ol}}) \int \left[f_{\text{sig}} \mathcal{P}_{\text{sig}}(\Delta t') R_{\text{sig}}(\Delta t_i - \Delta t') \right. \\
& + (1 - f_{\text{sig}}) \mathcal{P}_{\text{bkg}}(\Delta t') R_{\text{bkg}}(\Delta t_i - \Delta t') \Big] d(\Delta t') \\
& + f_{\text{ol}} P_{\text{ol}}(\Delta t_i),
\end{aligned} \tag{2}$$

where $P_{\text{ol}}(\Delta t)$ is a broad Gaussian function that represents an outlier component with a small fraction f_{ol} [9]. The width of the outlier component for DS-II is determined to be $(44 \pm 5)\ \text{ps}$; the fractions of the outlier components are $(3.1 \pm 1.2) \times 10^{-4}$ for events with the f_{tag} vertex reconstructed with more than one track, and $(1.2 \pm 0.1) \times 10^{-2}$ for the case only one track is used. These values are comparable to those for DS-I [9]. The signal probability f_{sig} depends on the r region and is calculated on an event-by-event basis as a function of p_B^{cms} for the $B^0 \rightarrow \phi K_L^0$ decay and as a function of ΔE and M_{bc} for the other modes. A PDF for background events, $\mathcal{P}_{\text{bkg}}(\Delta t)$, is modeled as a sum of exponential and prompt components, and is convolved with a sum of two Gaussians R_{bkg} . Parameters in $\mathcal{P}_{\text{bkg}}(\Delta t)$ and R_{bkg} for continuum background are determined by the fit to the Δt distribution for events outside the ΔE - M_{bc} signal region except for the $B^0 \rightarrow \phi K_L^0$ decay. For the $B^0 \rightarrow \phi K_L^0$ decay, we

use p_B^{cms} sideband events to obtain the parameters. Parameters in $\mathcal{P}_{\text{bkg}}(\Delta t)$ and R_{bkg} for $B\bar{B}$ background events in $B^0 \rightarrow \eta' K_S^0$, $B^0 \rightarrow K_S^0 \pi^0$ and $B^0 \rightarrow \phi K_L^0$ decays are determined from MC simulation.

We fix τ_{B^0} and Δm_d at their world average values [22]. We assume no CP asymmetry in the background Δt distributions and possible CP asymmetries in the B decay backgrounds are treated as sources of systematic error. In order to reduce the statistical error on \mathcal{A} , we include events without vertex information in the analysis of $B^0 \rightarrow K_S^0 \pi^0$. The likelihood value in this case is obtained by integrating Eq. (2) over Δt_i .

The only free parameters in the final fit are \mathcal{S} and \mathcal{A} , which are determined by maximizing the likelihood function $L = \prod_i P_i(\Delta t_i; \mathcal{S}, \mathcal{A})$ where the product is over all events. Table III summarizes the fit results of \mathcal{S} and \mathcal{A} . We define the raw asymmetry in each Δt bin by $(N_{q=+1} - N_{q=-1}) / (N_{q=+1} + N_{q=-1})$, where $N_{q=+1(-1)}$ is the number of observed candidates with $q = +1(-1)$ [23]. Figures 4(a-f) show the raw asymmetries in two regions of the flavor-tagging parameter r . While the numbers of signal events in the two regions are similar, the effective tagging efficiency is much larger and the background dilution is smaller in the region $0.5 < r \leq 1.0$. Note that these projections onto the Δt axis do not take into account event-by-event information (such as the signal fraction, the wrong tag fraction and the vertex resolution), which is used in the unbinned maximum-likelihood fit.

Tables IV and V list the systematic errors on \mathcal{S} and \mathcal{A} , respectively. The total systematic errors are obtained by adding each contribution in quadrature, and are much smaller than the statistical errors for all modes.

To determine the systematic error that arises from uncertainties in the vertex reconstruction, the track and vertex selection criteria are varied to search for possible systematic biases. Small biases in the Δz measurement are observed in $e^+e^- \rightarrow \mu^+\mu^-$ and other control samples. Systematic errors are estimated by applying special correction functions to account for the observed biases, repeating the fit, and comparing the obtained values with the nominal results. The systematic error due to the IP constraint in the vertex reconstruction is estimated by varying ($\pm 10\mu\text{m}$) the smearing used to account for the B flight length. Systematic errors due to imperfect SVD alignment are determined from MC samples that have artificial misalignment effects to reproduce impact-parameter resolutions observed in data.

Systematic errors due to uncertainties in the wrong tag fractions are studied by varying the wrong tag fraction individually for each r region. Systematic errors due to uncertainties in the resolution function are also estimated by varying each resolution parameter obtained from data (MC) by $\pm 1\sigma$ ($\pm 2\sigma$), repeating the fit and adding each variation in quadrature. Each physics parameter such as τ_{B^0} and Δm_d is also varied by its error. A possible fit bias is examined by fitting a large number of MC events.

Systematic errors from uncertainties in the background fractions and in the background Δt shape are estimated by varying each background parameter obtained from data (MC) by $\pm 1\sigma$ ($\pm 2\sigma$).

Additional sources of systematic errors are considered for B decay backgrounds that are neglected in the PDF. We consider uncertainties both in their fractions and CP asymmetries; for modes that have non-vanishing CP asymmetries, we conservatively vary the CP -violation parameters within the physical region and take the largest variation as the systematic error. The effect of backgrounds from $K^+K^-K_S^0$ and $f_0(980)K_S^0$ ($f_0(980) \rightarrow K^+K^-$) in the $B^0 \rightarrow \phi K_S^0$ sample is considered. Uncertainties from $B \rightarrow \phi K^*$ and other rare B decay backgrounds in the $B^0 \rightarrow \phi K_L^0$ sample are also taken into account. Effects of possible CP asymmetries

in B decay backgrounds for $K_S^0\pi^0$ and $f_0(980)K_S^0$ are evaluated. The peaking background fraction in the $B^0 \rightarrow f_0(980)K_S^0$ sample depends on the functions used in the fit to the $\pi^+\pi^-$ invariant mass distribution. The systematic errors due to the uncertainties of the masses and widths of the resonances used in the fit are estimated. The width of $f_0(980)$ is varied between $0.04 \text{ GeV}/c^2$ and $0.1 \text{ GeV}/c^2$. The mass and width of the $f_X(1300)$ are varied by $\pm 0.03 \text{ GeV}/c^2$ and $\pm 0.1 \text{ GeV}/c^2$, respectively. The effect of possible interference between resonant and non-resonant amplitudes, which is neglected in the nominal analysis, is also evaluated. We perform a fit to the $\pi^+\pi^-$ distribution of a MC sample generated with interfering amplitudes and phases for $B \rightarrow K\pi\pi$ decays measured from data [12]. The observed difference in the signal yield from the true value is taken into account in the systematic error determination. We also repeat the fit to the Δt distribution ignoring the contribution of the peaking background. The differences in \mathcal{S} and \mathcal{A} from our nominal results are included in the systematic error.

Finally, we investigate the effects of interference between CKM-favored and CKM-suppressed $B \rightarrow D$ transitions in the f_{tag} final state [24]. A small correction to the PDF for the signal distribution arises from the interference. We estimate the size of the correction using the $B^0 \rightarrow D^{*-}\ell^+\nu$ sample. We then generate MC pseudoexperiments and make an ensemble test to obtain systematic biases in \mathcal{S} and \mathcal{A} . In general, we find effects on \mathcal{S} are negligibly small, while there are sizable possible shifts in \mathcal{A} .

Various crosschecks of the measurements are performed. We reconstruct charged B meson decays that are the counterparts of the $B^0 \rightarrow f_{CP}$ decays and apply the same fit procedure. All results for the \mathcal{S} term are consistent with no CP asymmetry, as expected. Lifetime measurements are also performed for the f_{CP} modes and the corresponding charged B decay modes. The fits yield τ_{B^0} and τ_{B^+} values consistent with the world average values. MC pseudoexperiments are generated for each decay mode to perform ensemble tests. We find that the statistical errors obtained in our measurements are all consistent with the expectations from the ensemble tests.

For the $B^0 \rightarrow \phi K^0$ decay, a fit to DS-I alone yields $\mathcal{S} = -0.68 \pm 0.46(\text{stat})$ and $\mathcal{A} = 0.00 \pm 0.28(\text{stat})$, while a fit to DS-II alone yields $\mathcal{S} = +0.80 \pm 0.45(\text{stat})$ and $\mathcal{A} = +0.15 \pm 0.33(\text{stat})$. Note that the results for DS-I differ from our previously published results $\mathcal{S} = -0.96 \pm 0.50^{+0.09}_{-0.11}$ and $\mathcal{A} = -0.15 \pm 0.29 \pm 0.07$ [4], as the decays $B^0 \rightarrow \phi K_L^0$ and ϕK_S^0 ($K_S^0 \rightarrow \pi^0\pi^0$) are included in this analysis. Fit results to $B^0 \rightarrow \phi K_S^0$ ($K_S^0 \rightarrow \pi^+\pi^-$) decays in DS-I in this analysis are $\mathcal{S} = -0.97 \pm 0.50(\text{stat})$ and $\mathcal{A} = 0.15 \pm 0.29(\text{stat})$, which are consistent with the previous results. From MC pseudoexperiments, the probability that the difference between the \mathcal{S} values in DS-I and DS-II is larger than the observed difference (1.46) is estimated to be 4.5%. Fits to only ϕK_S^0 decays and only ϕK_L^0 decays yield $\mathcal{S} = 0.02 \pm 0.33$ and $\mathcal{A} = 0.07 \pm 0.22$, and $-\mathcal{S} = 2.3 \pm 2.0$ and $\mathcal{A} = 0.6 \pm 1.2$, respectively. A $\sin 2\phi_1$ measurement with DS-II is performed using $B^0 \rightarrow J/\psi K_S^0$ ($K_S^0 \rightarrow \pi^+\pi^-$ or $\pi^0\pi^0$) and $B^0 \rightarrow J/\psi K_L^0$ decays as a crosscheck. Applying the same procedure to both DS-I and DS-II, we obtain $\mathcal{S}_{J/\psi K^0} = +0.696 \pm 0.061(\text{stat})$ and $\mathcal{A}_{J/\psi K^0} = +0.011 \pm 0.043(\text{stat})$ for DS-I, and $\mathcal{S}_{J/\psi K^0} = +0.629 \pm 0.069(\text{stat})$ and $\mathcal{A}_{J/\psi K^0} = +0.035 \pm 0.044(\text{stat})$ for DS-II. The results are in good agreement with each other, and are also consistent with SM expectations. As all the other checks mentioned above also yield results consistent with expectations, we conclude that the difference in $\mathcal{S}_{\phi K^0}$ between the two datasets is due to a statistical fluctuation.

For the $B^0 \rightarrow \eta' K_S^0$, the statistical significance of the CP asymmetry is calculated with the Feldman-Cousins frequentist approach [25]. The case with no CP asymmetry ($\mathcal{S} = 0$ and $\mathcal{A} = 0$) is ruled out at 99.92% confidence level, equivalent to 3.4 standard deviations

for Gaussian errors.

As discussed in Section I, to a good approximation, the SM predicts $\mathcal{S} = -\xi_f \sin 2\phi_1$ for the $B^0 \rightarrow \phi K^0$, $f_0(980)K_S^0$, $\eta'K_S^0$, ωK_S^0 and $K_S^0\pi^0$ decays. For the $B^0 \rightarrow K^+K^-K_S^0$ decay, the SM prediction is given by $\mathcal{S} = -(2f_+ - 1) \sin 2\phi_1$. The effective $\sin 2\phi_1$ for this mode is obtained to be $0.74 \pm 0.27 \pm 0.06^{+0.38}_{-0.19}$. The third error is an additional systematic error arising from the uncertainty of the $\xi_f = +1$ fraction. Figure 5 summarizes the $\sin 2\phi_1$ determination based on our \mathcal{S} measurements for these decays. For each mode, the first error shown in the figure is statistical and the second error is systematic. We also include the result of the time-dependent CP -violating asymmetry measurement in $B^0 \rightarrow K_S^0 K_S^0 K_S^0$ decays by Belle [26]. We obtain $\sin 2\phi_1 = +0.40 \pm 0.13$ as a weighted average, where the error includes both statistical and systematic errors. The result differs from the SM expectation by 2.4 standard deviations.

IV. SUMMARY

We have performed improved measurements of CP -violation parameters for $B^0 \rightarrow \phi K^0$ (including both ϕK_S^0 and ϕK_L^0), $K^+K^-K_S^0$ and $\eta'K_S^0$ decays, and new measurements for $B^0 \rightarrow f_0(980)K_S^0$, ωK_S^0 and $K_S^0\pi^0$ decays. These charmless decays are dominated by $b \rightarrow s$ flavor-changing neutral currents and are sensitive to possible new CP -violating phases. The results for each individual decay mode are consistent with the SM expectation within two standard deviations except for the $B^0 \rightarrow f_0(980)K_S^0$ decay. The combined result for the $B^0 \rightarrow \phi K^0$, $K^+K^-K_S^0$, $f_0(980)K_S^0$, $\eta'K_S^0$, ωK_S^0 , $K_S^0\pi^0$ and previously reported $K_S^0 K_S^0 K_S^0$ decays differs from the SM expectation by 2.4 standard deviations. Measurements with a much larger data sample are required to conclusively establish the existence of a new CP -violating phase beyond the SM.

Acknowledgments

We thank the KEKB group for the excellent operation of the accelerator, the KEK cryogenics group for the efficient operation of the solenoid, and the KEK computer group and the National Institute of Informatics for valuable computing and Super-SINET network support. We acknowledge support from the Ministry of Education, Culture, Sports, Science, and Technology of Japan and the Japan Society for the Promotion of Science; the Australian Research Council and the Australian Department of Education, Science and Training; the National Science Foundation of China under contract No. 10175071; the Department of Science and Technology of India; the BK21 program of the Ministry of Education of Korea and the CHEP SRC program of the Korea Science and Engineering Foundation; the Polish State Committee for Scientific Research under contract No. 2P03B 01324; the Ministry of Science and Technology of the Russian Federation; the Ministry of Higher Education, Science and Technology of the Republic of Slovenia; the Swiss National Science Foundation; the National Science Council and the Ministry of Education of Taiwan; and the U.S. Department of Energy.

[1] A. G. Akeroyd *et al.*, hep-ex/0406071 and references therein.

- [2] See for example,
Y. Grossman and M. P. Worah, Phys. Lett. B **395**, 241 (1997); D. London and A. Soni, Phys. Lett. B **407**, 61 (1997); T. Moroi, Phys. Lett. B **493**, 366 (2000); D. Chang, A. Masiero and H. Murayama, Phys. Rev. D **67**, 075013 (2003); S. Baek, T. Goto, Y. Okada and K. Okumura, Phys. Rev. D **64**, 095001 (2001).
- [3] Throughout this paper, the inclusion of the charge conjugate decay mode is implied unless otherwise stated.
- [4] Belle Collaboration, K. Abe *et al.*, Phys. Rev. Lett. **91**, 261602 (2003).
- [5] BaBar Collaboration, B. Aubert *et al.*, Phys. Rev. D **71**, 111102(R) (2005); Phys. Rev. D **71**, 091102(R) (2005); Phys. Rev. Lett. **94**, 191802 (2005); Phys. Rev. Lett. **94**, 041802 (2005)
- [6] M. Kobayashi and T. Maskawa, Prog. Theor. Phys. **49**, 652 (1973).
- [7] A. B. Carter and A. I. Sanda, Phys. Rev. D **23**, 1567 (1981); I. I. Bigi and A. I. Sanda, Nucl. Phys. **B193**, 85 (1981).
- [8] Belle Collaboration, K. Abe *et al.*, Phys. Rev. Lett. **87**, 091802 (2001); Phys. Rev. D **66**, 032007 (2002); Phys. Rev. D **66**, 071102 (2002).
- [9] Belle Collaboration, K. Abe *et al.*, Phys. Rev. D **71**, 072003 (2005).
- [10] BaBar Collaboration, B. Aubert *et al.*, Phys. Rev. Lett. **89**, 201802 (2002); Phys. Rev. Lett. **94**, 161803 (2005)
- [11] J. Alexander *et al.* (Heavy Flavor Averaging Group), hep-ex/0412073.
- [12] Belle Collaboration, A. Garmash *et al.*, Phys. Rev. D **69**, 012001 (2004); Belle Collaboration, K. Abe *et al.*, Belle-CONF-0410 (2004).
- [13] S. Kurokawa and E. Kikutani, Nucl. Instrum. Methods Phys. Res., Sect. A **499**, 1 (2003), and other papers included in this volume.
- [14] Belle Collaboration, A. Abashian *et al.*, Nucl. Instrum. Methods Phys. Res., Sect. A **479**, 117 (2002).
- [15] Y. Ushiroda (Belle SVD2 Group), Nucl. Instrum. Methods Phys. Res., Sect. A **511**, 6 (2003).
- [16] Belle Collaboration, K. Abe *et al.*, Phys. Rev. Lett. **87**, 101801 (2001).
- [17] ARGUS Collaboration, H. Albrecht *et al.*, Phys. Lett. B **241**, 278 (1990).
- [18] Belle Collaboration, K. Abe *et al.*, Phys. Rev. Lett. **91**, 261801 (2003).
- [19] T. Skwarnicki, Ph.D. Thesis, Institute for Nuclear Physics, Krakow 1986; DESY Internal Report, DESY F31-86-02 (1986).
- [20] H. Kakuno *et al.*, Nucl. Instrum. Methods Phys. Res., Sect. A **533**, 516 (2004).
- [21] H. Tajima *et al.*, Nucl. Instrum. Methods Phys. Res., Sect. A **533**, 370 (2004).
- [22] S. Eidelman *et al.*, Phys. Lett. B **592**, 1 (2004).
- [23] We use an alternative definition of the raw asymmetry, $(N_{q\xi_f=-1} - N_{q\xi_f=+1})/(N_{q\xi_f=-1} + N_{q\xi_f=+1})$, for the decay $B^0 \rightarrow \phi K^0$ to take the opposite CP parities for the decays $B^0 \rightarrow \phi K_S^0$ and ϕK_L^0 into account.
- [24] O. Long, M. Baak, R. N. Cahn and D. Kirkby, Phys. Rev. D **68**, 034010 (2003).
- [25] G. J. Feldman and R. D. Cousins, Phys. Rev. D **57**, 3873 (1998).
- [26] Belle Collaboration, K. Sumisawa *et al.*, hep-ex/0503023.

TABLE I: Event fractions ϵ_l , wrong-tag fractions w_l , wrong-tag fraction differences Δw_l , and average effective tagging efficiencies $\epsilon_{\text{eff}}^l = \epsilon_l(1 - 2w_l)^2$ for each r interval for DS-II. Errors for w_l and Δw_l include both statistical and systematic uncertainties. The event fractions are obtained from $J/\psi K_S^0$ data.

l	r interval	ϵ_l	w_l	Δw_l	ϵ_{eff}^l
1	0.000 – 0.250	0.397 ± 0.015	0.464 ± 0.007	$+0.008 \pm 0.007$	0.002 ± 0.001
2	0.250 – 0.500	0.146 ± 0.009	0.320 ± 0.008	-0.022 ± 0.010	0.019 ± 0.002
3	0.500 – 0.625	0.108 ± 0.008	0.225 ± 0.011	$+0.029 \pm 0.011$	0.033 ± 0.004
4	0.625 – 0.750	0.107 ± 0.008	0.158 ± 0.010	$+0.003 \pm 0.011$	0.050 ± 0.005
5	0.750 – 0.875	0.098 ± 0.007	0.109 ± 0.009	-0.028 ± 0.011	0.060 ± 0.005
6	0.875 – 1.000	0.144 ± 0.009	0.015 ± 0.005	$+0.007 \pm 0.007$	0.135 ± 0.009

TABLE II: Estimated signal purities and signal yields N_{sig} in the signal region for each f_{CP} mode that is used to measure CP asymmetries. The result for the $B^0 \rightarrow K_S^0 \pi^0$ decay is obtained with the sample after flavor tagging but before vertex reconstruction. The results for other decays are obtained after flavor tagging and vertex reconstruction.

Mode	ξ_f	purity	N_{sig}
ϕK_S^0	-1	0.63	139 ± 14
ϕK_L^0	+1	0.17	36 ± 15
$K^+ K^- K_S^0$	+1 (83%), -1 (17%)	0.56	398 ± 28
$f_0(980) K_S^0$	+1	0.53	94 ± 14
$\eta' K_S^0$	-1	0.61	512 ± 27
ωK_S^0	-1	0.56	31 ± 7
$K_S^0 \pi^0$ (high- $\mathcal{R}_{s/b}$)	-1	0.54	168 ± 16
$K_S^0 \pi^0$ (low- $\mathcal{R}_{s/b}$)	-1	0.15	79 ± 19

TABLE III: Results of the fits to the Δt distributions. The first error is statistical and the second error is systematic. We combine $B^0 \rightarrow \phi K_S^0$ and $B^0 \rightarrow \phi K_L^0$ decays to obtain $\mathcal{S}_{\phi K^0}$ and $\mathcal{A}_{\phi K^0}$.

Mode	SM expectation for \mathcal{S}	\mathcal{S}	\mathcal{A}
ϕK^0	$+\sin 2\phi_1$	$+0.08 \pm 0.33 \pm 0.09$	$+0.08 \pm 0.22 \pm 0.09$
$K^+ K^- K_S^0$	$-(2f_+ - 1)\sin 2\phi_1$	$-0.49 \pm 0.18 \pm 0.04$	$-0.09 \pm 0.12 \pm 0.07$
$f_0(980) K_S^0$	$-\sin 2\phi_1$	$+0.47 \pm 0.41 \pm 0.08$	$-0.39 \pm 0.27 \pm 0.09$
$\eta' K_S^0$	$+\sin 2\phi_1$	$+0.65 \pm 0.18 \pm 0.04$	$-0.19 \pm 0.11 \pm 0.05$
ωK_S^0	$+\sin 2\phi_1$	$+0.76 \pm 0.65^{+0.13}_{-0.16}$	$+0.27 \pm 0.48 \pm 0.15$
$K_S^0 \pi^0$	$+\sin 2\phi_1$	$+0.32 \pm 0.61 \pm 0.13$	$-0.11 \pm 0.20 \pm 0.09$

TABLE IV: Summary of the systematic errors on \mathcal{S} .

	ϕK^0	$K^+ K^- K_S^0$	$f_0(980) K_S^0$	$\eta' K_S^0$	ωK_S^0	$K_S^0 \pi^0$
Vertex reconstruction	0.01	0.01	0.02	0.01	0.01	0.02
Flavor tagging	0.01	< 0.01	0.01	0.01	0.04	0.01
Resolution function	0.04	0.03	0.03	0.03	0.07	0.05
Physics parameters	< 0.01	< 0.01	0.01	< 0.01	0.01	0.02
Possible fit bias	0.01	0.01	0.03	0.01	$^{+0.01}_{-0.10}$	0.02
Background fraction	0.08	0.02	0.05	0.02	0.10	0.08
Background Δt shape	0.01	< 0.01	0.04	< 0.01	0.02	0.08
Tag-side interference	< 0.01	< 0.01	< 0.01	< 0.01	0.01	< 0.01
Total	0.09	0.04	0.08	0.04	$^{+0.13}_{-0.16}$	0.13

TABLE V: Summary of the systematic errors on \mathcal{A} .

	ϕK^0	$K^+ K^- K_S^0$	$f_0(980) K_S^0$	$\eta' K_S^0$	ωK_S^0	$K_S^0 \pi^0$
Vertex reconstruction	0.03	0.04	0.04	0.03	0.04	0.04
Flavor tagging	< 0.01	< 0.01	0.01	0.01	< 0.01	0.01
Resolution function	0.02	0.02	0.02	0.01	0.04	< 0.01
Physics parameters	< 0.01	< 0.01	< 0.01	< 0.01	< 0.01	< 0.01
Possible fit bias	0.01	0.01	0.03	0.01	$^{+0.01}_{-0.03}$	0.01
Background fraction	0.04	0.01	0.06	0.02	0.14	0.04
Background Δt shape	0.03	< 0.01	0.01	< 0.01	0.03	0.05
Tag-side interference	0.06	0.06	0.04	0.03	0.03	0.05
Total	0.09	0.07	0.09	0.05	0.15	0.09

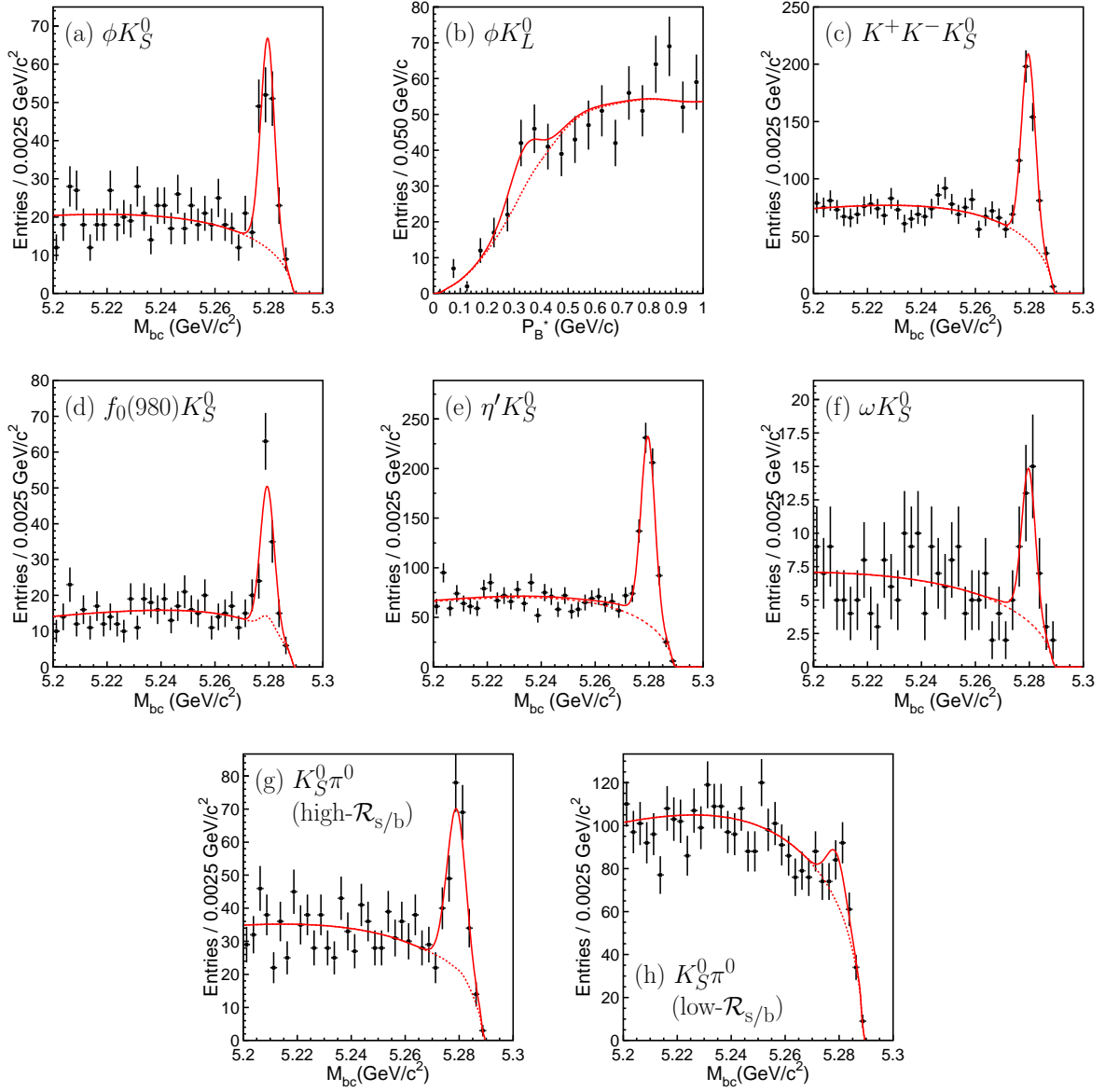


FIG. 1: M_{bc} distributions for (a) $B^0 \rightarrow \phi K_S^0$, (c) $B^0 \rightarrow K^+ K^- K_S^0$, (d) $B^0 \rightarrow f_0(980) K_S^0$, (e) $B^0 \rightarrow \eta' K_S^0$, (f) $B^0 \rightarrow \omega K_S^0$, (g) $B^0 \rightarrow K_S^0 \pi^0$ (high- $\mathcal{R}_{s/b}$), and (h) $B^0 \rightarrow K_S^0 \pi^0$ (low- $\mathcal{R}_{s/b}$), within the ΔE signal region and (b) p_B^{cms} distribution for $B^0 \rightarrow \phi K_L^0$. Solid curves show the fits to signal plus background distributions, and dashed curves show the background contributions.

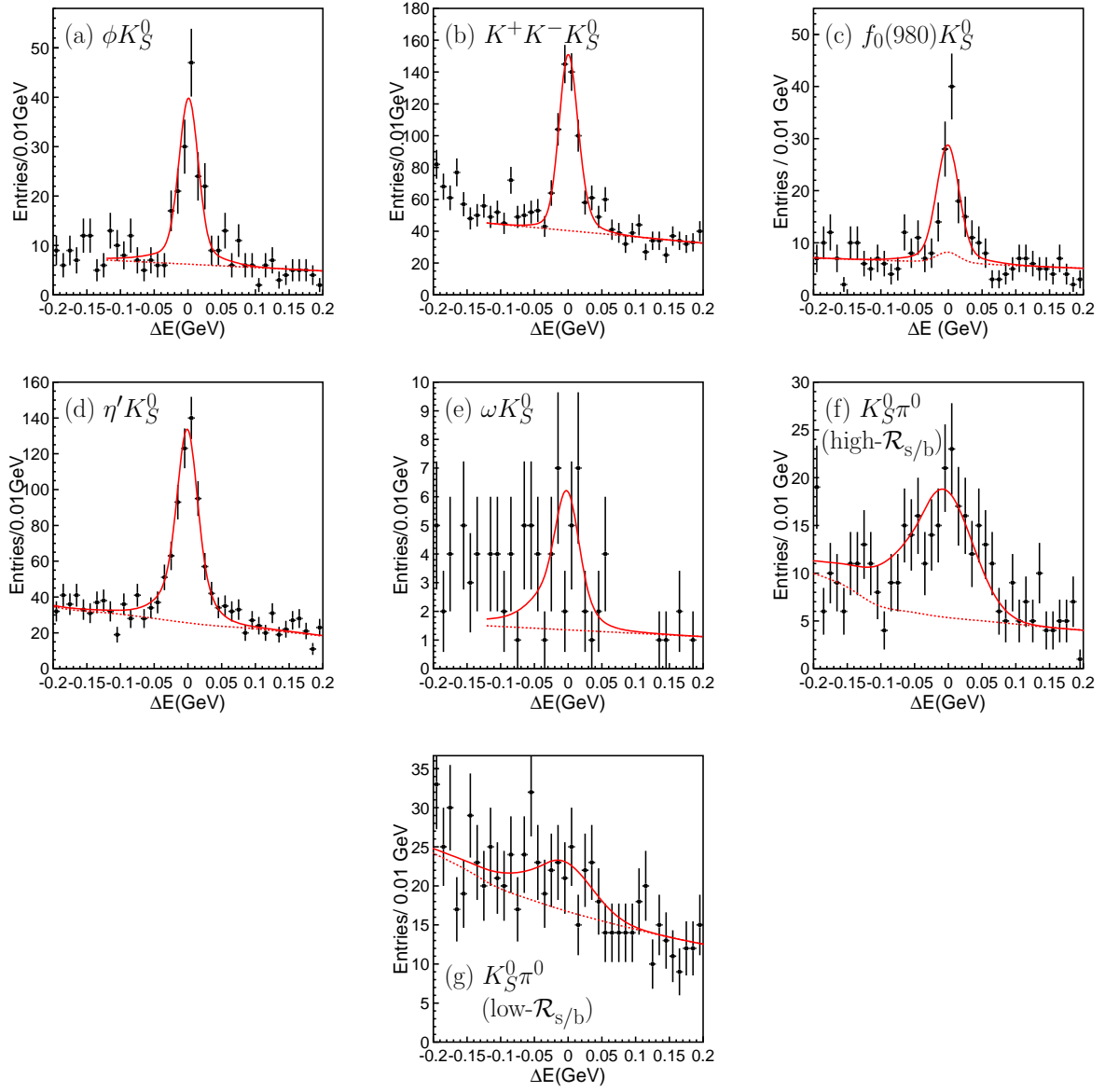


FIG. 2: ΔE distributions for (a) $B^0 \rightarrow \phi K_S^0$, (b) $B^0 \rightarrow K^+ K^- K_S^0$, (c) $B^0 \rightarrow f_0(980) K_S^0$, (d) $B^0 \rightarrow \eta' K_S^0$, (e) $B^0 \rightarrow \omega K_S^0$, (f) $B^0 \rightarrow K_S^0 \pi^0$ (high- $\mathcal{R}_{s/b}$), and (g) $B^0 \rightarrow K_S^0 \pi^0$ (low- $\mathcal{R}_{s/b}$), within the M_{bc} signal region. Solid curves show the fit to signal plus background distributions, and dashed curves show the background contributions.

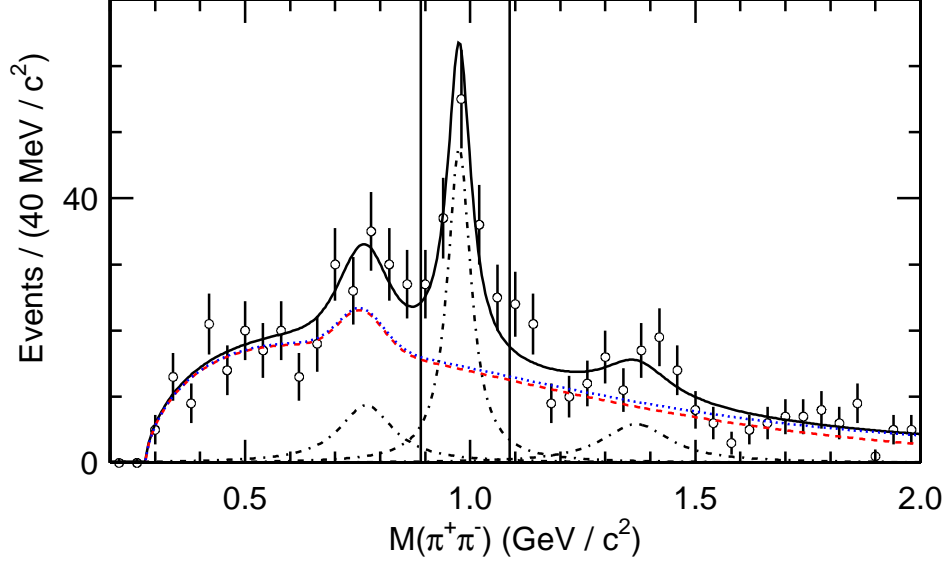


FIG. 3: Invariant mass distribution of $\pi^+\pi^-$ pairs for $B^0 \rightarrow f_0(980)K_S^0$ candidates in the ΔE - M_{bc} signal region. The solid curve shows the fit result. The dashed line shows continuum background. The dotted line shows the sum of the continuum and the non-resonant $B^0 \rightarrow \pi^+\pi^-K_S^0$. The dot-dashed lines show the $B^0 \rightarrow \rho^0 K_S^0$ (left), the $B^0 \rightarrow f_0(980)K_S^0$ (middle), and the $B^0 \rightarrow f_X(1300)K_S^0$ (right).

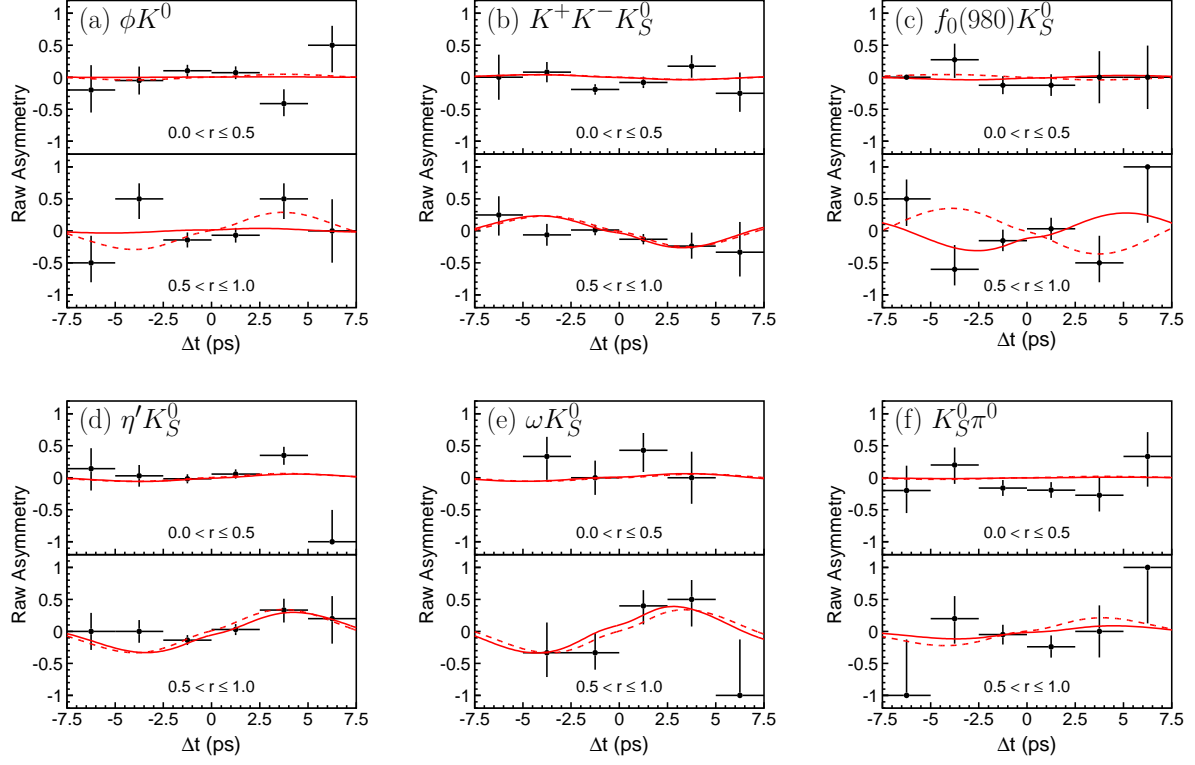


FIG. 4: Raw asymmetry in each Δt bin with $0 < r \leq 0.5$ (top) and with $0.5 < r \leq 1.0$ (bottom) for (a) $B^0 \rightarrow \phi K^0$, (b) $B^0 \rightarrow K^+ K^- K_S^0$, (c) $B^0 \rightarrow f_0(980) K_S^0$, (d) $B^0 \rightarrow \eta' K_S^0$, (e) $B^0 \rightarrow \omega K_S^0$, and (f) $B^0 \rightarrow K_S^0 \pi^0$. The solid curves show the results of the unbinned maximum-likelihood fits. The dashed curves show the SM expectation with $\sin 2\phi_1 = +0.73$ and $\mathcal{A} = 0$.

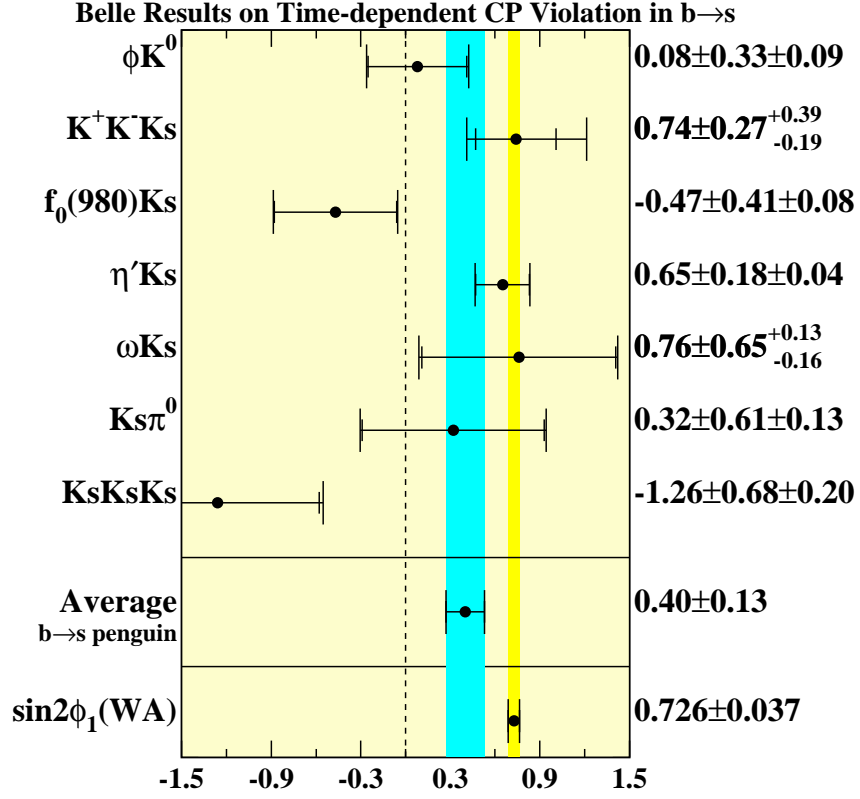


FIG. 5: Summary of $\sin 2\phi_1$ measurements performed with hadronic B^0 decays governed by the $b \rightarrow s\bar{q}q$ transition. The world average $\sin 2\phi_1$ value obtained from $B^0 \rightarrow J/\psi K^0$ and other related decay modes governed by the $b \rightarrow c\bar{c}s$ transition [11] is also shown as the SM reference.